TOTAL RESISTANCE PREDICTION OF *SELF PROPELLED COAL BARGE* (SPCB) USING *COMPUTATIONAL FLUID DYNAMIC*

Agung Purwana[1)], Adi Wirawan Husodo[1)]

[1)]Marine Engineering Department, Politeknik Perkapalan Negeri Surabaya, Indonesia
Email: agpurwana@gmail.com, adi_wirawan@ppns.ac.id

Abstract

In the present paper the *computational fluid dynamic* (CFD) technique is applied to predict the total resistance (Rt) of *Self Propelled Coal Barge* (SPCB). The simulation process was executed using ANSYS®software based on fluid flow (CFX) solver. The selected CFD method is *volume of fluid* (VOF). The solid modeling of SPCB is developed using Maxsurf®. Boundary conditions are set on each domain area covering *bottom*,*free surface*, *inlet*, *outlet*, *ship*and *wall*. The variation of computaitional grid (*meshing grid*) which is used in computation are SST (*Shear Stress Transport*)67,000, SST 73,000, SST 103,000, SST 117,000, SST 127,000, SST 147,000, SST 157,000, and SST 200,500. Total resistance (Rt) resulted from CFX computation is validated with total resistance (Rt) resulted from Holtrop. The larger of grid meshing size, the better of validation result. The CFD technique demonstrated good agreement with *Holtrop* formulae in predicting the total resistance (Rt) of SPCB.

Kata kunci: *CFD, total resistance, meshing grid, shear stress transport, volume of fluid (VOF)*

1. INTRODUCTION

The use of SPCB (*Self Propelled Coal barge*) for coal distriution in Indonesia continue to increase. Similar with commonly SPB (*Self Propelled barge*), SPCB has no familiar hull form according to mostly merchant ships. The changing from no engine driven to be engine driven pushes the designer to optimize the hull form of SPCB. The optimized hull form of SPCB will result the optimum total resistance (Rt).

This research studied the application of CFD technique to predict the total resistance (Rt) of SPCB. The problems which have been studied are SPCB solid modelling, boundary conditions of domain, optimum grid meshing and validation of total resistance (Rt) resulted from CFD computation with total resistance (Rt) resulted from *Holtrop* formulae.

2. LITERATURE STUDY

2.1. CFD Application on Ship Resistance Calculation

CFD technique has been widely used in ship preliminary design, especially for the case of merchant ship (*low/medium speed*). The studies focused on how to estimate the total resistance (Rt) directly [1,4,8,9,10,11], and also focused on how to optimize the hull form to reduce the total resistance as well drag [2,3,5,6,7].

Ahmed Y, et al.[1] performed numerical simulation to determine the incompressible free surfaceflow around a VLCC hull form. A commercial viscous flow finite volumecode using the two-phase *Eulerian–Eulerian* fluid approach and a potential flow code based on the*Rankine* source method have been used in their study. The simulation conditions are the ones for whichexperimental results exist. The *shear stress transport* (SST) turbulence model has been used in theviscous flow code. A tetrahedral unstructured grid was used with the viscous flow code for meshing thecomputational domain, while quadrilateral structural patches were used with the potential flow codefor meshing the VLCC hull surface and

the water surface around it. The results compare well with theavailable experimental data and they allow an understanding of the differences that can be expectedfrom viscous and potential flow methods as a result of their different mathematical formulations, whichmake their complementary application useful for determining the total ship resistance.

Zhang[2] optimized the hull form of ship especially at forward partin order to minimize the wave making resistance. *Rankine source method* was combined with CFD technique.

*Kim*and*Yang*[3]developed the effective and efficient hull form of ship based on CFD optimization. They used 2 (two) techniques; radial interpolation function and curve of sectional area. Both techniques have implemented to container type of ship. According to their analysis results, it could be concluded that both techniques could minimize drag effectively and efficient.

Ahmed, Y.M. [4] simulated numerically the free surface flow around DTMB 5414 complex hull form with different Froude number. The simulation used RANSE *code* that available at CFX. The method used here is *volume of fluid method* (VOM). ICEM CFD Grid Generator is used to develop the *hybrid grid*. It would be used as RANSE code solver. The simulation results are then verified by experiment results. According to simulation results, the use of *hybrid mesh* combined with RANSE *code* solver has the significant advantages. Even with small computation source (small meshing grid), the free surface flow could be well predicted. The *potential flow method* could be used to determine wave making resistance and wave pattern. While the *viscous flow method* could predict the frictional resistance and viscous pressure component in every variance of velocities.

Park and *Choi*[5,6] developed the ship's hull form to get minimum wave making resistance of medium speed *Ro-pax* by using *genetic algorithm optimization method* combined with NURBS based automatic hull form modification method. They also used the *sequential quadratic programming* numerical optimization. The ship model was based on series-60 model. The frictional resistance is estimated with ITTC 1957 *model-ship correlation*, while the wave making resistance is calculated using *potential-flow panel method*. During optimization process, hull surface modelling is performed using *B-spline surface model*. The simulation result is validated using optimized model towing test result. There is significant reduction of total resistance (13%). Specific for the *residuary resistance*, the reduction is 40%.

Zhang[7]also optimized the hull form of ship based on Series-60 model to get the better performance of resistance. The resistance performance of three optimized models (SGA, NGA, NLP) is analyzed, and the results are then compared to that of source model. The chosen optimization method is *Rankine Source Method*. According to analysis, the Rankine Source method is very suitable to use in the first stage of ship design. There is significant reduction of both total resistance and wave making resistance. For NGA model, the reductions are 11.4% for total resistance and 31.2% for wave making. For SGA model, the reductions are 8.0% for total resistance and 24.4% for wave making. And for NLP model, the reductions are 5.5% for total resistance and 18.8% for wave making.

Chrismanto D, et al. [8]studied the influence of CFD variables to calculate the ship resistance coefficients. The variables here are domain dimensions, meshing dimensions and boundary conditions. The magnitudes of three variables above arethen being variated. The aim of simulation is to get the closest ship resistance coefficient compared to the experiment result.

Samarpana K, et al. [9] investigated the *free surface flow* around ship hull based on technical computation in order to calculate the ship resistance. According to [9], the better meshing size, the more compatible the relation of meshing size and turbulence model or *wall function*. Furthermore, ship resistance calculation using CFD has good agreement with ship resistance resulted both from *Holtrop* and towing test.

Ali A, et al. [10]performed the simulation to predict the *wave making resistance* and *flow pattern* around hull of catamaran (with and

without fin stabilizer) using CFD. The chosen CFD method is *volume of fluid flow*. The analysis uses the *Reynold Average Navier Stoke* (RANS) especially related how to solve the problems of free surface effect. At both model configurations, the investigation is performed at 10 to 20 knots speed and uses the *k-epsilon* turbulence model. The simulation results are *pressure resistance* (Rp) and *flow pattern*.

Chrismanto D, et al.[11]also used the CFD technique to investigate the shape of forward part in order to get the smallest ship resistance. [11] used the variation of *Froude Number* (Fn). [11] also proved that CFD technique results the better calculation than the previous techniques.

2.2. Ship Resistance

Ship resistance is defined as force used to tow the ship at given speed in smooth or calm water condition (*towing force*) [12]. If there are no appendage constructions attached, the ship resistance resulted is *bare-hull resistance*. According to *Holtrop* [12], total ship resistance (Rt) is calculated using Equation (1).

$$R_T = \frac{1}{2}\rho V^2 S_{tot}\left[C_F(1+k) + C_A\right] + \frac{R_w}{W}W \qquad (1)$$

Equation (1) shows that the ship resistance is composed of *viscous resistance* (*Rv*) and *wave making resistance* (*Rw*). *Rv*can be calculated using Equation (2) and (3) and *Rw* is calculated using Equation (4).

$$R_V = \frac{1}{2}\rho V^2 C_{FO}(1+k_1)S \qquad (2)$$

$$R_V = \frac{1}{2}\rho V^2 C_{FO}(1+k)S_{tot} \qquad (3)$$

$$\frac{R_W}{W} = C_1 C_2 C_3 e^{m_1 Fn^d} + m_2\, cos(\lambda Fn^{-2}) \qquad (4)$$

Equation (2) is used to calculate *Rv*without *appendages*,and Equation (3) is used to calculate *Rv*with *appendages*. C_{FO}, the *friction resistance coefficient*, is calculated using ITTC 1957 formulae. See Equation (5).

$$C_{FO} = \frac{0.075}{(\log Rn - 2)^2} \qquad (5)$$

2.3. General Fluid Dynamic Equations

The general equations of fluid flow represent mathematical statements of the conservation laws of physics, such that: fluid mass is conserved, the rate of change of momentum equals the sum of the forces on a fluid particle, and the rate of change of energy is equal to the sum of the rate of heat addition to and the rate of work done on a particle. The governing equations for an unsteady, three dimensional, compressible viscous flows are [13]:

$$\frac{\partial \rho}{\partial t} + \nabla \cdot (\rho U) = 0 \qquad (6)$$

$$\frac{\partial(\rho u)}{\partial t} + \nabla \cdot (\rho u U) = -\frac{\partial p}{\partial x} + \frac{\partial \tau_{xx}}{\partial x} + \frac{\partial \tau_{yx}}{\partial y} + \frac{\partial \tau_{zx}}{\partial z} + \rho f_x \qquad (7)$$

$$\frac{\partial(\rho v)}{\partial t} + \nabla \cdot (\rho v U) = -\frac{\partial p}{\partial y} + \frac{\partial \tau_{xy}}{\partial x} + \frac{\partial \tau_{yy}}{\partial y} + \frac{\partial \tau_{zy}}{\partial z} + \rho f_y \qquad (8)$$

$$\frac{\partial(\rho w)}{\partial t} + \nabla \cdot (\rho w U) = -\frac{\partial p}{\partial w} + \frac{\partial \tau_{xz}}{\partial x} + \frac{\partial \tau_{yz}}{\partial y} + \frac{\partial \tau_{zz}}{\partial z} + \rho f_z \qquad (9)$$

$$\frac{\partial}{\partial t}\left(\rho\left(e+\frac{U^2}{2}\right)\right)+\nabla\cdot\left(\rho U\left(e+\frac{U^2}{2}\right)\right) \quad (10)$$
$$=\rho\dot{q}+\frac{\partial}{\partial x}\left(k\frac{\partial T}{\partial x}\right)+\frac{\partial}{\partial y}\left(k\frac{\partial T}{\partial y}\right)+\frac{\partial}{\partial z}\left(k\frac{\partial T}{\partial z}\right)-\frac{\partial(up)}{\partial x}-\frac{\partial(vp)}{\partial y}-\frac{\partial(wp)}{\partial z}+\frac{\partial(u\tau_{xx})}{\partial x}+\frac{\partial(u\tau_{yx})}{\partial y}+\frac{\partial(u\tau_{zx})}{\partial z}+\frac{\partial(u\tau_{xy})}{\partial x}+\frac{\partial(u\tau_{yy})}{\partial y}+\frac{\partial(u\tau_{zy})}{\partial z}+\frac{\partial(u\tau_{xz})}{\partial x}+\frac{\partial(u\tau_{yz})}{\partial y}+\frac{\partial(u\tau_{zz})}{\partial z}+\rho fU$$

Equation (6) is Continuity Equation, Equation (7) to (9) are Momentum Equation for *x-y-z*components, and Equation (10) is Energy Equation. Where: ρ is the fluid density, U = (*u, v, w*) the fluid velocity, *p* the pressure, *T* the temperature, *e* is the internal energy per unit mass, *f* = (*fx, fy, fz*) is a body force, *k* is the thermal conductivity, $\dot{q}$is the rate of volumetric heat addition per unit mass and τ_{nn} are the viscous stresses.

In mostly hydrodynamic analysis, the flow is assumed as incompressible and Newtonian. The viscosity is constant throughout the flow [13]. Then the Equation (6) becomes:

$$\nabla\cdot U=0 \quad (11)$$

And the Equations (7) to Equation (9) become:

$$\rho\frac{Du}{Dt}=-\frac{\partial p}{\partial x}+\mu\nabla^2u+\rho\cdot f_x \quad (12)$$

$$\rho\frac{Dv}{Dt}=-\frac{\partial p}{\partial y}+\mu\nabla^2v+\rho\cdot f_y \quad (13)$$

$$\rho\frac{Dw}{Dt}=-\frac{\partial p}{\partial z}+\mu\nabla^2w+\rho\cdot f_z \quad (14)$$

Where D/Dt is the substantial derivative given by:

$$\frac{D}{Dt}=\frac{\partial}{\partial t}+u\frac{\partial}{\partial x}+v\frac{\partial}{\partial y}+w\frac{\partial}{\partial z} \quad (15)$$

The continuity and momentum equations are now de-coupled from the energy equation and are all that is necessary to solve for the velocity and pressure fields in an incompressible flow [13].

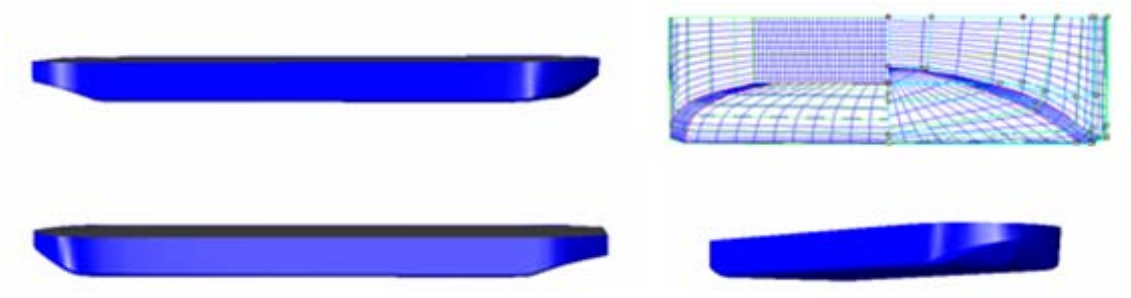

Figure 1. SPCB Model

3. METHODOLOGY

3.1. SPCB-Existing Modeling

Principal particulars of SPCB used in this research are shown in Table 1 [14].

Table 1. Principal Particulars of SPCB [14]

Principal Particulars	Spec.	Unit
Loa	91.5	m
Lpp	90.0	m
B	24.0	m
H	7.0	m
T	5.0	m
Displacement	9951.85	ton
	9709.12	m^3

Solid modeling of SPCB is performed using Maxsurf®. The modeling result can be shown in Figure 1. To validate the model SPCB resulted from Maxsurf®, we compared the principal particulars of SPCB modeling to those of SPCB

data (Table 1). The validation results can be shown in Table 2. The maximum deviation is 0.26%. Furthermore, the SPCB model resulted from Maxsurf® can be used for further analysis.

Table 2. Validation of Principal Particulars

Principal Particulars	Unit	Data	Modeling	Dev
Loa	M	91.5	91.6	0.11%
Lpp	M	90.0	90	0.00%
B	M	24.0	23.988	- 0.05%
H	M	7.0	7.0	0.00%
T	M	5.0	5.0	0.00%
Displacement	ton	9951.85	9926.35	- 0.26%
	m^3	9709.12	9684.24	- 0.26%

3.2. Boundary Conditions

Dimension of domains affect to the computation process. Dimension of domain will accommodate the free surface motion [15]. ANSYS® CFX *Design Modeler* is used to model the dimensions of domain. Figure 2 shows the dimensions domain used in simulation. The coordinates of SPCB model are laid at AP (horizontal coordinate) and DWL (vertical coordinate). Main deck construction has been added to SPCB model to make it solid. The solid requirement of model will help in defining the fluid surface.

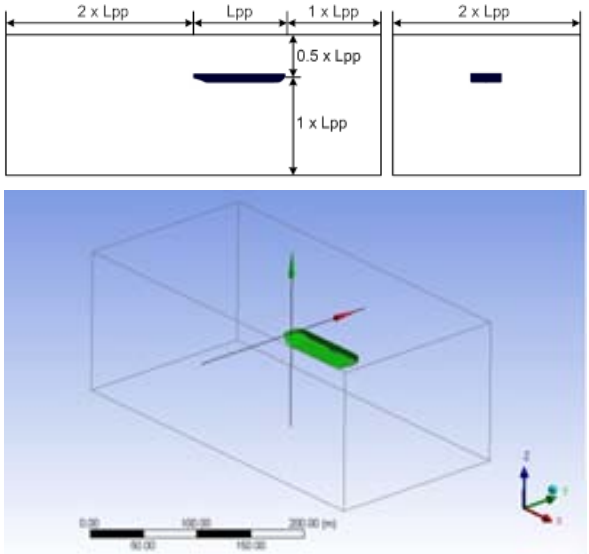

Figure 2. Dimensions of Domain

After domain dimensions have been defined, the meshing process would be executed. The boundary conditions of computation used here are *bottom, free, inlet, outlet, ship* and *wall*. In the *inlet* area, the considered parameter is fluid velocity (air and water). The fluid velocity used in the validation process is set to 5.144 m/s (service velocity). In the *outlet* area, the parameter which is considered is *static pressure*. The *top* and *bottom* area are considered as *free sleep wall*. Turbulence model that is used is *Shear Stress Transport* (SST).The setting of boundary condition and meshing result can be shown in Figure 3.

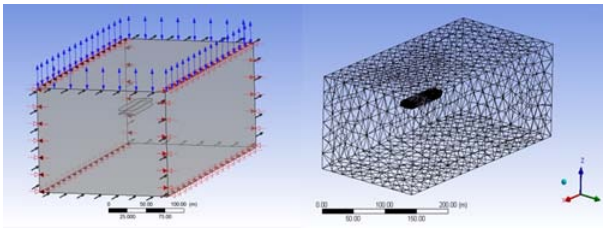

Figure 3. Boundary Condition and Meshing Computation

In the first step of computation, validation process is executed to find the optimum grid meshing for 10 knot (5.144 m/sec) velocity of service. The chosen mesh type is *unstructured mesh* with computer's *default* dimension of mesh. Before running, the iteration process for all basic dynamic equation of CFD is executed until convergent condition is achieved. In this research, convergent condition is achieved if an RMS criterion reaches the targeted value (1×10^{-5}). Characteristic of pressure interpolation is *linear*, while characteristic of velocity is *trilinear*. Figure 4 shows the iteration process to find convergent condition. This process is executed for seven different grid meshes.

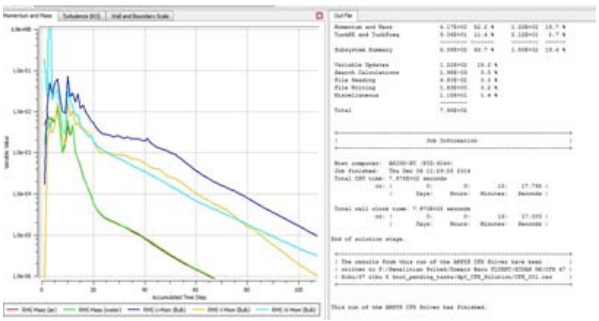

Figure 4. Iteration for Convergent Condition

The result of validation shows that the best grid mesh is 200,500 SST. However, it is not the optimum grid mesh if it compared to the Rt resulted by Holtrop for 10 knot (0.5144 m/sec) velocity. The iteration process stopped at 200,500

SST due to computer specification.However, according to linear extrapolation, the grid mesh optimum is around 340,000 SST.

Table 3. Grid Mesh Validation Result compared to R_THoltrop at 10 knot (5.144 m/sec)

Grid Mesh (x 1000)	Rt_{CFX}(kN)	$Rt_{Holtrop}$ (kN)	Error
67	267.748	180.23	32.687%
103	251.748	180.23	28.409%
117	248.48	180.23	27.467%
127	250.056	180.23	27.924%
147	238.938	180.23	24.570%
157	234.433	180.23	23.121%
200.5	225.863	180.23	20.204%

4. ANALYSIS

The variations of SPCB velocity of service used in this research are 2.5 knot, 5 knot, 7.5 knot, 8 knot and 10 knot.

At 2.5 knot velocity of service and 200,500 SST grid mesh the time need to achieve the convergent condition is 1967 sec. The magnitude of velocity ranged from 0.084 m/sec to 1.37 m/sec (Figure 5). While the magnitude of pressure ranged from 2.926 x 10^5 Pa ~ 2.972 x 10^5 Pa. (Figure 6). The total resistance (Rt) resulted from simulaton is 14.12 kN.

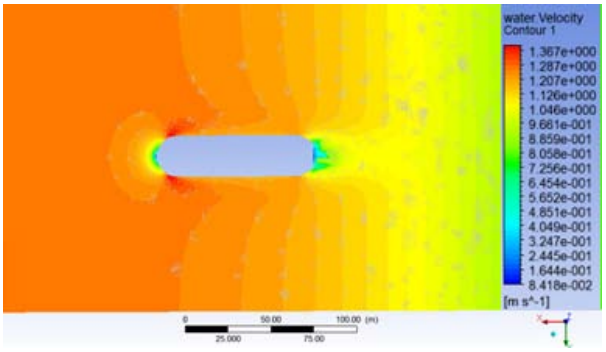

Figure 5. Velocity Contour at Vs 2.5 knots

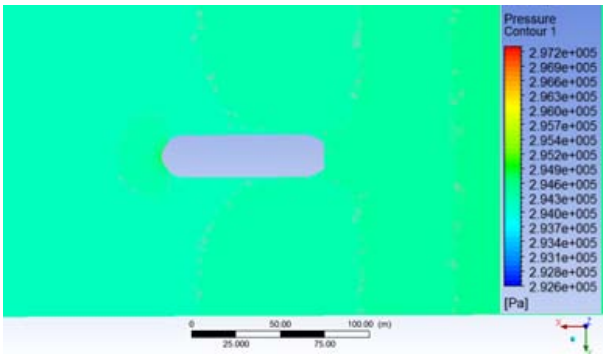

Figure 6. Pressure Contour at Vs 2.5 knots

At 5 knot velocity of service and 200,500 SST grid mesh, the time need to achieve the convergent condition is 1766 sec. The magnitude of velocity ranged from 0.168 m/sec to 2.73 m/sec (Figure 7). While the magnitude of pressure ranged from 2.933 x 10^5 Pa ~ 2.984 x 10^5 Pa (Figure 8). The total resistance (Rt) resulted from simulaton is 56.49 kN.

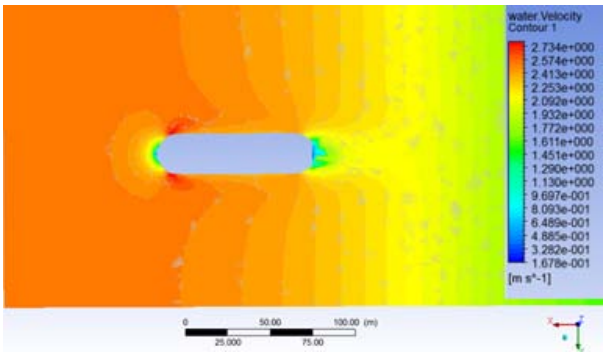

Figure 7. Velocity Contour at Vs 5 knots

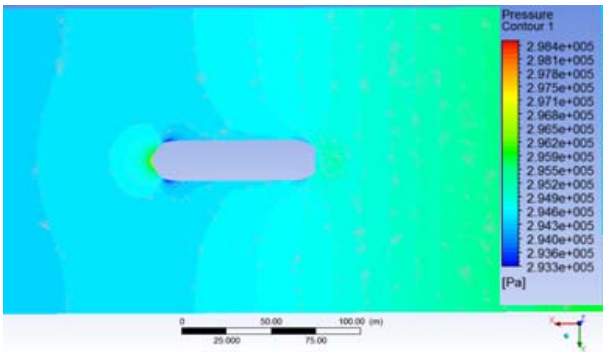

Figure 8. Pressure Contour at Vs 5 knots

At 7.5 knot velocity of service and 200,500 SST grid mesh, the time need to achieve the convergent condition is 2010 sec. The magnitude of velocity ranged from 0.25 m/sec to 4.1 m/sec (Figure 9). While the magnitude of pressure ranged from

2.922 x 10^5 Pa ~ 3.004 x 10^5 Pa (Figure 10). The total resistance (Rt) resulted from simulaton is 104.49 kN.

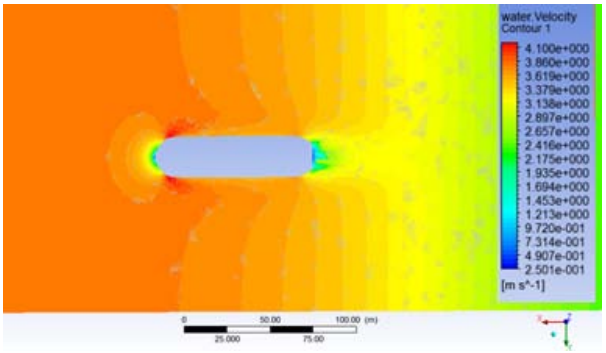

Figure 9. Velocity Contour at Vs 7.5 knots

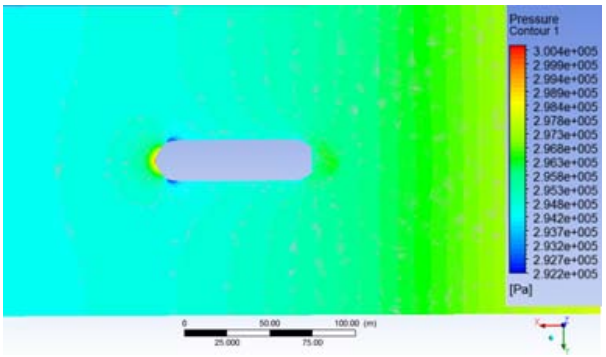

Figure 10. Pressure Contour at Vs 7.5 knots

At 8 knot velocity of service and 200,500 SST grid mesh, the time need to achieve the convergent condition is 1549 sec. The magnitude of velocity ranged from 0.25 m/sec to 4.373 m/sec (Figure 11). While the magnitude of pressure ranged from 2.919 x 10^5 Pa ~ 3.009 x 10^5 Pa (Figure 12). The total resistance (Rt) resulted from simulaton is 117.72 kN.

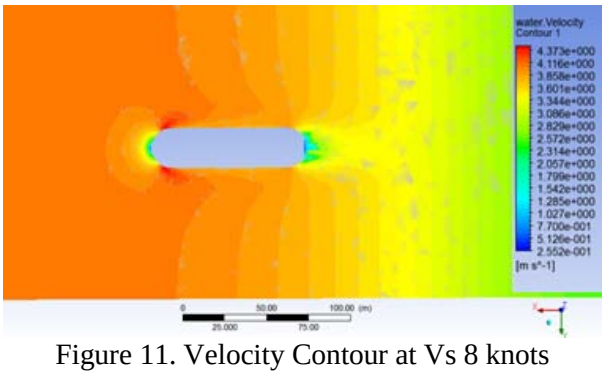

Figure 11. Velocity Contour at Vs 8 knots

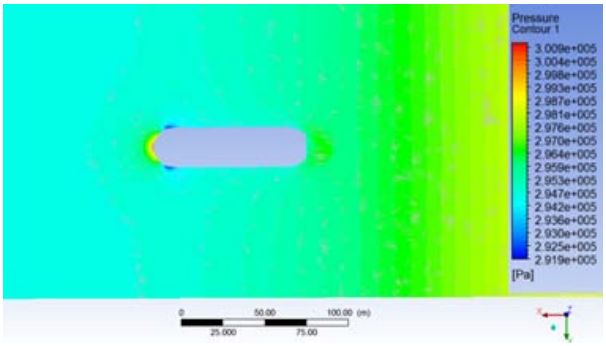

Figure 12. Pressure Contour at Vs 8 knots

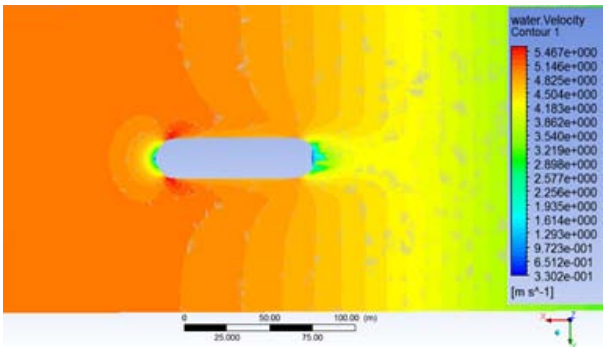

Figure 13. Velocity Contour at Vs 10 knots

At 10 knot velocity of service and 200,500 SST grid mesh, the time need to achieve the convergent condition is 1477 sec. The magnitude of velocity ranged from 0.330 m/sec to 5.467 m/sec (Figure 13). While the magnitude of pressure ranged from 2.906 x 10^5 Pa ~ 3.035 x 10^5 Pa (Figure 14). The total resistance (Rt) resulted from simulaton is 225.86 kN.

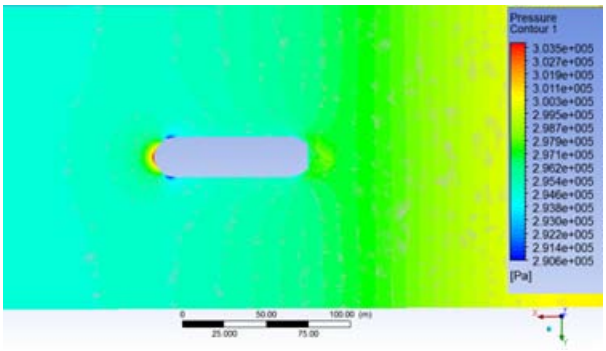

Figure 14. Pressure Contour at Vs 10 knots

According to velocity contour and pressure contour (Figure 5 to Figure 14), the flow velocity at *inlet* side is the same with SPCB velocity. The flow velocity is then going to decrease to the lowest value when reaches the fore-hull of SPCB.

The flow velocity reaches the maximum value when passing through the area where the boundary layer is initially developed (bigger than velocity at *inlet* side).At alongside of hulland in the direction away from hull, the value of flow velocity decreases and equals to the *inlet* flow velocity. It proves the *divergent wave principles* of wave making resistance [16]. After through the aft-hull, the flow velocity becomes varying. At center line of aft-hull, the flow velocity decreases to the lowest point. At portside and starboard side of aft-hull, the flow velocity increases until *outlet* area. The magnitude of pressure is inversely proportional to the flow velocity. The pressure increases to maximum number when reaches the fore-hull of SPCB. When passing through the area where the boundary layer created, the pressure becomes decrease to the lowest value. At alongside of hull and in the direction away from hull, the value of pressure increases. After through the aft-hull of SPCB the pressure values become varying. At center line of aft-hull, the pressure increases to the maximum. At portside and starboard side of aft-hull, the pressure decreases until *outlet* area.

The results of total resistance (Rt) calculation using CFX simulation and Holtrop are shown in Table 4. According to Table 4, the CFX computation at 200,500 SST grid mesh could calculate the total resistance (Rt) of SPCB proportionally if compared to those which is calculated by Holtrop formulae.

Table 4. Validation of Total Resistance (Rt) based on CFX Simulation and Holtrop.

V (knots)	V (m/s)	Rt_{CFX} (kN)	$Rt_{Holtrop}$ (kN)	Error (%)
0	0.000	NS	0.00	0.000
1	0.514	NS	2.38	
2	1.029	9.03642	8.83	2.284
2.5	1.286	14.1195	13.45	4.742
3	1.543	NS	18.96	
4	2.058	36.1547	32.53	10.026
5	2.572	56.4937	49.34	12.663
6	3.086	81.1653	69.21	14.730
7	3.601	NS	92.01	
7.5	3.858	127.102	104.49	17.790
8	4.115	145.477	117.72	19.080
9	4.630	NS	146.76	
10	5.144	225.863	180.23	20.204

NS: Not Simulated

Figure 15 shows the pattern of SPCB Total Resistance (Rt) according to Table 4. Furthermore, the CFX simulation results show the good agreement with Holtrop Formulae. Even for velocity 2.5 knot to 10 knots still shows the error bigger than 5%. To solve such kind of problem is using better specification of computer. As information, this simulation executed using 4 RAM computers.

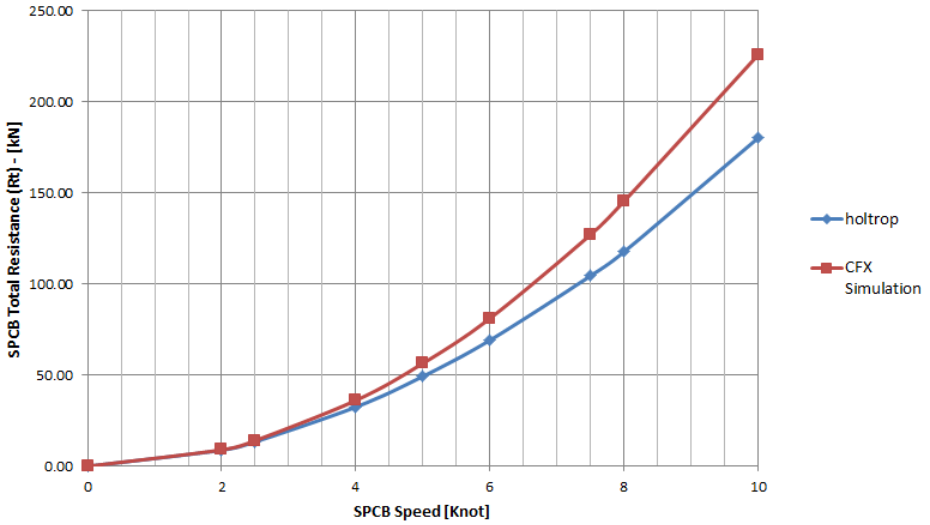

Figure 15. Total Resistance CFX Simulation Vs Holtrop

5. CONCLUSIONS

In the present study, unstructured meshing technique combined with SST (*Shear Stress Transport*) method was employed to predict the SPCB Total Resistance. Validation process was performed to get the best grid mesh dimension used in the simulation.

The simulation results were compared with the numerical results (Holtrop formulae). For all performance, the CFD simulation is depend on the technical specification of computer, especially in the selection of grid meshing and meshing type. Furthermore, the CFD simulation results have good agreement with numerical results.

REFERENCES

[1] Ahmed, Y., Soares, C.G.,"Simulation of Free Surface Flow Around a VLCC Hull Using Viscous and Potential Flow Methods", *Ocean Engineering*, Vol. 36, pp. 691–696, 2009.

[2] Zhang, B.J., "The Optimization of the Hull Form with the Minimum Wave Making Resistance Based on Rankine Source Method", Journal of Hydrodynamics, Vol. 21 (2), pp. 277-284, 2009.

[3] Kim, H., Yang, C., "A New Surface Modification Approach for CFD-Based Hull Form Optimization", 9th International Conference on Hydrodynamics, Shanghai, China, October 11-15, pp. 520-525, 2010.

[4] Ahmed, Y.M., "Numerical Simulation for the Free Surface Fow around a Complex Ship Hull Form at Different Froude Numbers", Alexandria Engineering Journal, Vol. 50, pp. 229-235, 2011.

[5] Park, D.W., Choi, H.J., "Study for Optimal Hull Form Design of a High Speed Ro-Pax Ship on Wave-making Resistance Performance", *Journal of Navigation and Port Research*, Vol. 36 (10), pp. 787-793, 2012, (in Korean).

[6] Park, D.W., Choi, H.J., "Hydrodynamic Hull Form Design Using an Optimization Technique", *International Journal of Ocean System Engineering*, Vol. 3 (1), pp. 1-9, 2013.

[7] Zhang, B.J., "Research on Optimization of Hull Lines for Minimum Resistance Based on Rankine Source Method", *Journal of Marine Science and Technology*, Vol. 20 (1), pp. 89-94, 2012.

[8] Chrismianto, D., Manik, P., "Studi PengaruhVariabel-variabel dalam CFD untuk Menghitung Koefisien Tahanan Kapal", Jurnal TEKNIK, Vol. 34 (3), pp. 182-187, 2013.

[9] Samarpana, K., Konapala, A., Ramesh, D., "Computational Investigation of Free Surface Flow around a Ship Hull", International Journal of Application or Innovation in Engineering & Management (IJAIEM), Vol. 2 (5), pp. 98-107, 2013.

[10] Ali, A., Maimun, A., Ahmed, Y.M., "Numerical Simulation on Wave Interference of Catamaran with Fin Stabilizer", JurnalTeknologi, Vol. 66(2), pp. 163–167, 2014.

[11] Chrismianto, D., Trimulyono, A., Hidayat, M.N., "Analisa Pengaruh Modifikasi Bentuk Haluan Kapal terhadap Hambatan Total dengan Menggunakan CFD", Jurnal KAPAL, Vol. 11 (1), pp. 40-48, 2014.

[12] Manen, V.J.D., Oossanen, V., edited by Lewis, E.V., "Principle of Naval Architecture Second Revision, Vol. II: Resistance, Propulsion and Vibration", Chapter V, SNAME, New Jersey, 1988.

[13] WS Atkins Consultants & members of the NSC, "Best Practice Guidelines for Marine Applications of Computational Fluid Dynamics".

[14] Murtedjo, M., Sambodho, K., Suntoyo, Rohani, I., "Analisis Sistem Distribusi Batu bara dari Coal Mining Hingga Coal Mother Vessel di Provinsi Kalimatan Tengah", *Laporan Penelitian Program Hibah Penelitian Laboratorium*, LPPM – ITS, 2013.

[15] Seo, J.H., Seol, D.M., Lee, J.H., Rhee, S.H., "Flexible CFD Meshing Strategy for Prediction of Ship Resistance and Propulsion Performance", *International Journal of Naval Architecture and Ocean Engineering*, Vol. (2), pp. 139-145, 2010.

[16] Van Manen, J.D., Van Oossanen, edited by Lewis, E.V., "Principle of Naval Architecture Second Revision", *Vol. II: Resistance, Propulsion and Vibration, Chapter V*, SNAME, New Jersey, 1988